Supplementary Material: Transport in Stark Many Body Localized Systems

Guy Zisling,[1] Dante M. Kennes,[2,3] and Yevgeny Bar Lev[1]

[1] *Department of Physics, Ben-Gurion University of the Negev, Beer-Sheva 84105, Israel*
[2] *Institute for Theory of Statistical Physics, RWTH Aachen University, and JARA Fundamentals of Future Information Technology, 52056 Aachen, Germany*
[3] *Max Planck Institute for the Structure and Dynamics of Matter, Center for Free Electron Laser Science, Luruper Chaussee 149, 22761 Hamburg, Germany*

I. TRANSITION LOCATION

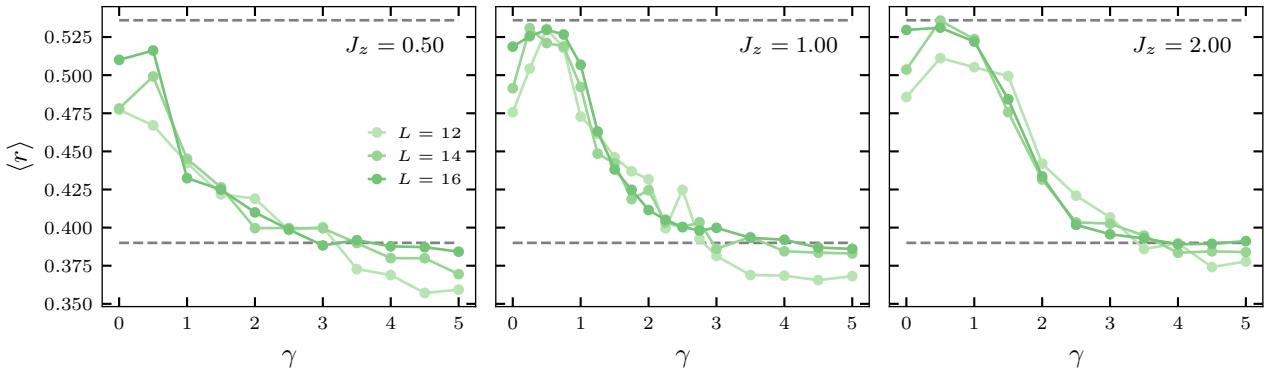

Figure S1. $\langle r \rangle$ as of a function of electric field strength for various interaction strengths (different panels), and system sizes. Larger system size corresponds to stronger color intensity. The black dashed lines correspond to WD statistics ($r \simeq 0.536$) and Poisson ($r \simeq 0.39$) statistics. The model parameters that were used are $J_{xy} = 2,\ J_z \in [0.5, 1, 2],\ \alpha = 0.5$.

To approximately assess the location of the Stark-MBL transition we use the standard metric,

$$r_\alpha = \min\left(\frac{s_\alpha}{s_{\alpha-1}}, \frac{s_{\alpha-1}}{s_\alpha}\right), \tag{S1}$$

where $s_\alpha \equiv E_{\alpha+1} - E_\alpha$ are the spacing between adjacent eigenvalues of the Hamiltonian. For integrable systems the mean of this quantity ($\langle r \rangle$), is typically given by $\langle r \rangle \approx 0.39$, which corresponds to a Poissonian distribution, while for quantum chaotic systems it is $\langle r \rangle \approx 0.536$, which corresponds to Wigner Dyson distribution. In Fig. S1 we examine $\langle r \rangle$ as a function of the electric field strength γ for various couplings J_z. We observe a transition from a Wigner-Dyson distribution for low electric fields to a Poissonian distribution at high electric fields. The transition occurs approximately at $\gamma \approx J_z$. This analysis does not depend strongly on the size of the system, in contrast to the mean-square displacement results presented in the main text. The middle panel ($J_z = 1$) is in agreement with Ref. [44] although we have used a different mechanism to break the symmetries of the model.

II. DELOCALIZATION TIME EXTRACTION

In Fig. S2 we present the analysis used to obtain $t^\star(\gamma, L)$ in Fig. 3 in the main text. The mean-square displacement (MSD) shows severe finite size effects, with subdiffusive behavior delayed to later times for larger system sizes. The locations of the plateaus (green horizontal lines) are calculated by taking the mean of the MSD between the 2nd and the 3rd peaks of the MSD. We fit the late time behavior with a power-law fit, $x^2 \propto t^a$ (orange dashed lines), and estimate the delocalization time $t^\star(\gamma, L)$ by the intersection of the plateaus with the power-law fits (orange crosses).

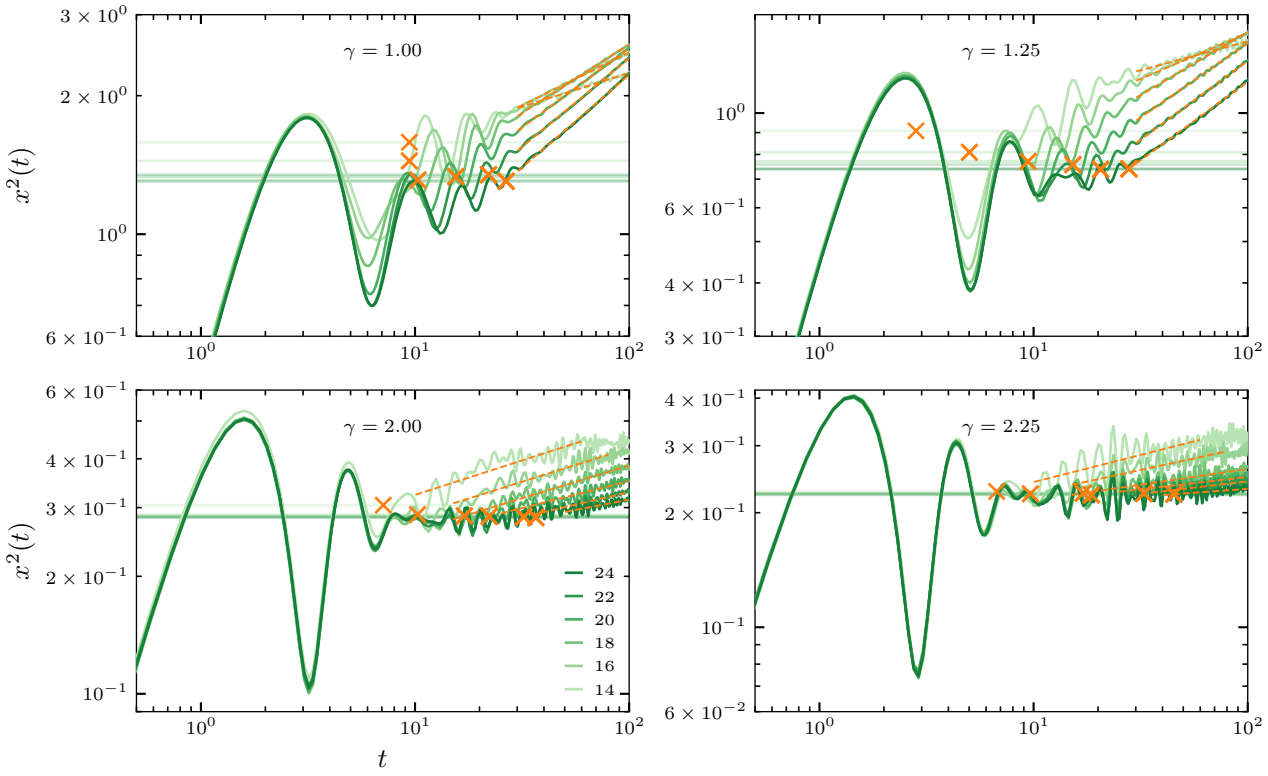

Figure S2. Mean-square displacement (MSD) as a function of time for $L \in [14, 24]$ (Krylov based method). The orange dashed line correspond to power-law fits ($x^2 \sim t^a$), while the horizontal lines indicate the plateau of the MSD calculated by taking the mean of the MSD between the 2nd and the 3rd peaks. The orange crosses are the estimated delocalization time $t^\star(\gamma, L)$ obtained from the intersection of the power-law fits with the plateau. The color of the plateau lines matches the coloring of the corresponding system size. All plots were obtained using $J_{xy} = 2,\ J_z = 1$.

III. FINITE-SIZE SUBDIFFUSIVE BEHAVIOR

From the power law-fits in Fig. S2 we can obtain the dynamical exponent a, which corresponds to the late-time growth of the MSD, $x^2 \sim t^a$. We plot this exponent as a function of the electric field γ and for various system sizes in Fig. S3. One can see an apparent transition between a subdiffusive behavior ($a < 1$) to a localized behavior ($a \sim 0$), with very strong finite-size effects.While for $\gamma > J_z$ the exponent seems to converge with the size of the system, it is important to keep in mind that the onset of the subdiffusive transport is pushed to later times for larger system sizes, as one can see in the main text and in Fig. S2 indicating that the observed subdiffusive behavior is a finite-size effect.

IV. SENSITIVITY TO BOUNDARY CONDITIONS

In this Section we show that the conclusions of the main text are robust to changes in the gauge and the boundary conditions. In Fig. S4 we have calculated the MSD as a function of time, using the dynamical gauge, (3) in the main text for various electric fields γ (rows), various system sizes (color intensity), and two different boundary conditions (columns). We see that in the dynamic gauge the MSD shows less pronounced oscillations compared to the static gauge, allowing to spot the formation of the localization plateau already for $\gamma = 1$. The results remain qualitatively the same to the results in the static gauge (Fig.S2), with severe finite size effects, and a delocalization time that is increasing with the system size. The quantitative difference between open and periodic boundary conditions serves as another indication of finite-size effects, though the localization plateau for both boundary conditions appears at about the same MSD.

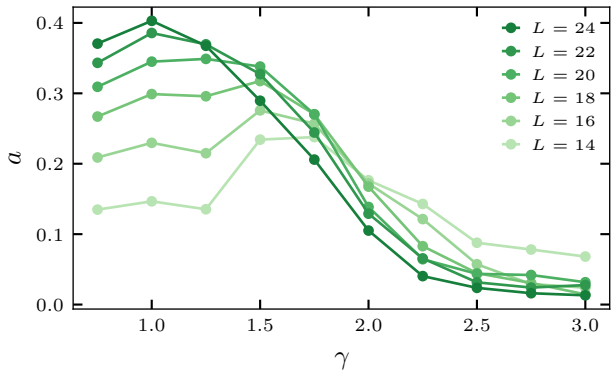

Figure S3. The dynamical exponent a as obtained from the fits to the MSD, $x^2 \propto t^a$ (see Fig. S2), as function of γ for various system sizes ($L \in [14, 24]$).

V. DYNAMICAL BEHAVIOR OF TRUNCATED EFFECTIVE HAMILTONIANS

In this Section we study the late-times dynamical behavior of the effective Hamiltonians calculated using Magnus expansion in γ^{-1} up to some order n. In Fig. S5 (left column) we calculate the MSD for two electric fields (rows). We see that it develops a pronounced linear behavior, indicative of diffusion, $x^2 \sim 2Dt$, where D is the linear response diffusion coefficient. For even longer times the MSD saturates, since the system is finite. We extract the diffusion coefficient from the relevant time windows (black dashed lines in Fig. S5), and plot it as a function of the truncation order, n on the right column of Fig. S5.

The diffusion coefficient $D(\gamma, n)$ is monotonically decreasing with the order of the Magnus expansion and the strength of the electric field, approximately following $D \sim 1/n$. While this finding indicates that the truncated effective Hamiltonian is delocalized, it doesn't imply much on the original interacting Stark model, since the diffusive behavior of the effective Hamiltonian emerges for at times for which the dynamics under the effective Hamiltonian doesn't *not* well approximate the numerically exact dynamics. What is interesting, is that the infinite order Magnus expansion, if it is convergent, could correspond to localized dynamics.

VI. CONVERGENCE CRITERIA OF THE MAGNUS EXPANSION

In this Section we examine the convergence of the Magnus expansion of the effective Hamiltonian,

$$\hat{H}_{\text{eff}}^{(n)} = \sum_{k=0}^{n} \hat{H}_k, \tag{S2}$$

while each term $\hat{H}_k$ is of the order of γ^{-k}. The D'Alembert criterion of convergence is $\left\|\hat{H}_{k+1}\right\| / \left\|\hat{H}_k\right\| < 1$, where $\|.\|$ indicates the operator norm. In Fig. S6 we the D'Alembert criterion is presented for different electric fields, γ. We see that while for $\gamma \leq 2$ the series is divergent, for $\gamma \gtrsim 3$ is it convergent at least up to 10th order. We note that this doesn't necessarily mean that the series has a finite radius of convergence, since divergence can occur for relatively large expansions orders [74].

VII. DENSITY OF STATES OF THE TRUNCATED EFFECTIVE HAMILTONIANS

The zero order truncated effective Hamiltonian, $\hat{H}_{\text{eff}}^{(0)}$ in (S2) corresponds to the interaction term,

$$\hat{H}_{\text{eff}}^{(0)} = J_z \sum_{i=1}^{L} \hat{S}_i^z \hat{S}_{i+1}^z, \tag{S3}$$

whose spectrum is composed of equally spaced degenerate bands, separated $J_z/4$ apart. The following terms of the expansion are of order J_z/γ, and they partially lift this degeneracy giving a width of J_z/γ to the bands. To

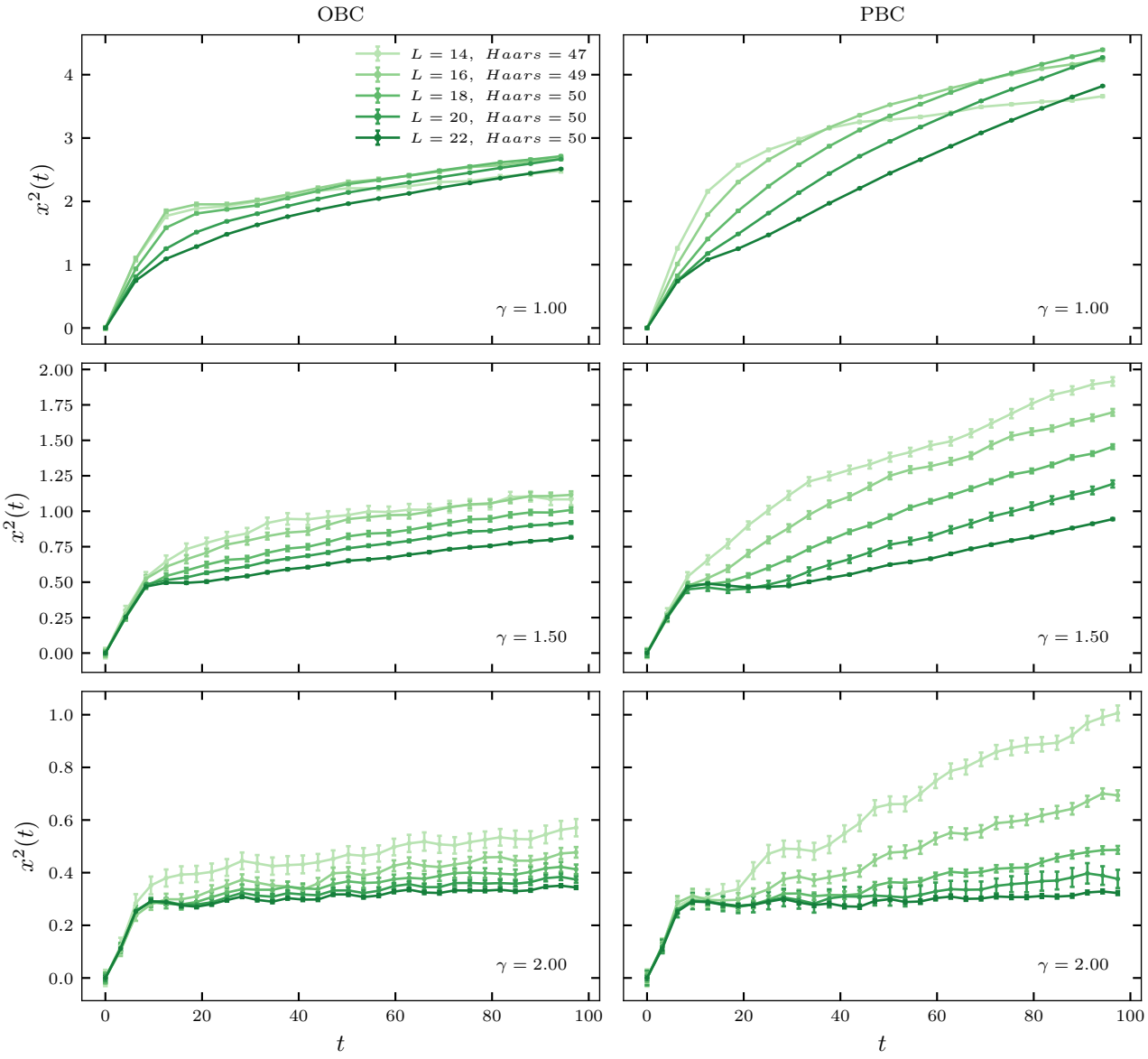

Figure S4. Mean-square displacement (MSD) as a function of time for $L \in [14, 24]$ (Krylov based method) calculated from the dynamic gauge (3) in the main text. Left column: open boundary conditions (OBC). Right column: periodic boundary conditions (PBC). Different rows have different electric fields $\gamma \in [1, 1.5, 2]$. All plots were obtained for $J_{xy} = 2,\ J_z = 1$.

demonstrate this in Fig. S7 we plot the density of states (DOS) of $\hat{H}^{(n)}_{\text{eff}}$ for a number of electric fields, γ. While the gaps are washed away for $J_z/4 < J_z/\gamma$, namely $\gamma < 4$, they become clearly visible as γ increases.

VIII. FINITE-SIZE ANALYSIS

In Fig. S8 we repeat the analysis of Fig. 4 from the main text for a number of system sizes, showing that there are no considerable system size dependence in the determination of t_{Magnus}, namely the time up to which there is a reasonable agreement between the MSD computed using $\hat{H}^{(n)}_{\text{eff}}$ and the MSD of the dynamical gauge Hamiltonian (3) in the main text.

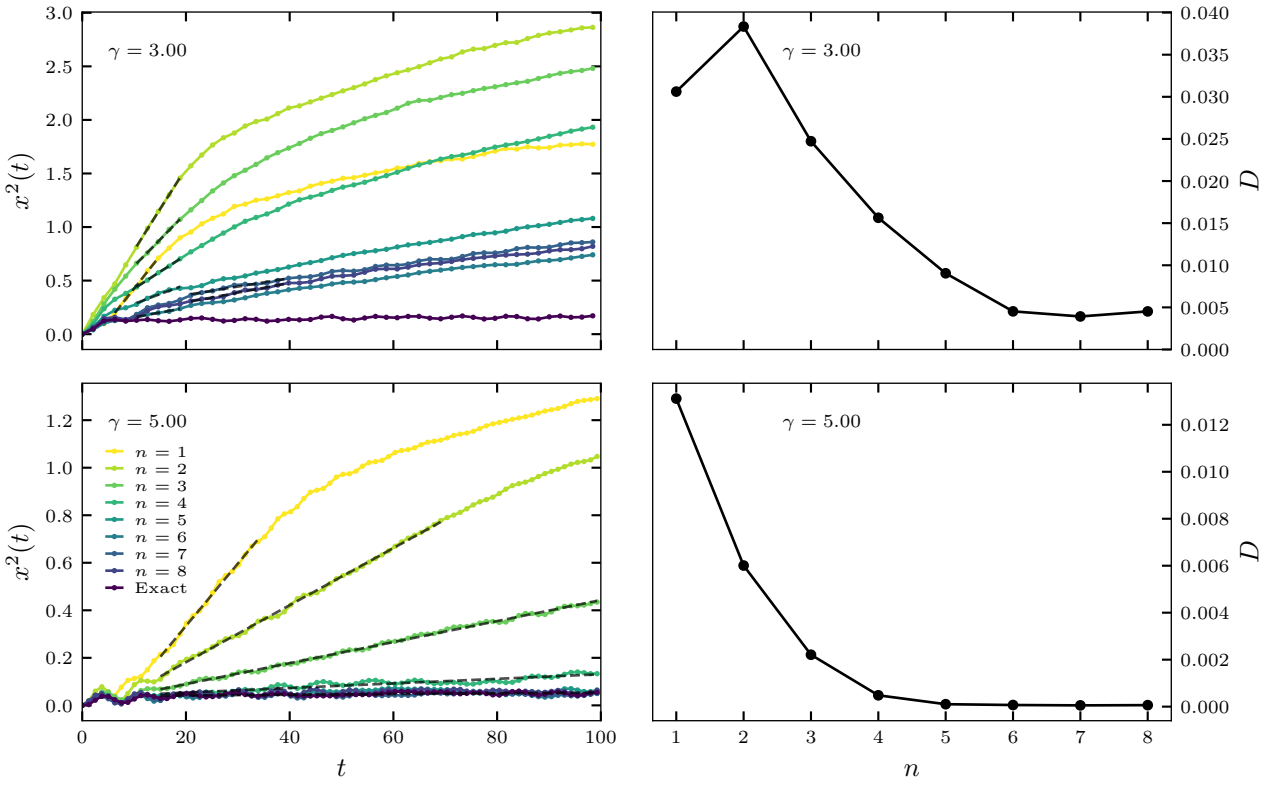

Figure S5. Mean-squared displacement as a function of time for two electric fields (left column). The darkest lines correspond to numerically exact results obtained using (Eq. 3 in the main text). The colored lines with increasing intensity corresponds to evolution using effective Hamiltonians (S2), obtained from a truncated Magnus expansion. The black dashed lines corresponds to linear fits, $x^2 \sim 2D\,t$, and the diffusion coefficient D is plotted in the right column as function of the truncation order. For both $\gamma = 3, 5$ there is a visible trend of $D \propto 1/n$. The parameters used are, $J_{xy} = 2,\ J_z = 1,\ L = 14$.

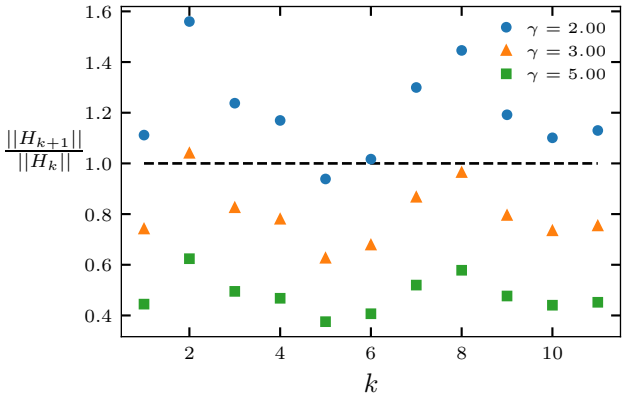

Figure S6. D'Alembert criterion of convergence as a function of the Magnus expansion order (k), $\left\|\hat{H}_{k+1}\right\| / \left\|\hat{H}_k\right\| < 1$ (see (S2) for definition). Different colors (markers) represents different electric field strength $\gamma = 2, 3$ and 5. The dashed black line corresponds to a convergence requirement.. The parameters used are, $J_{xy} = 2,\ J_z = 1,\ L = 10$.

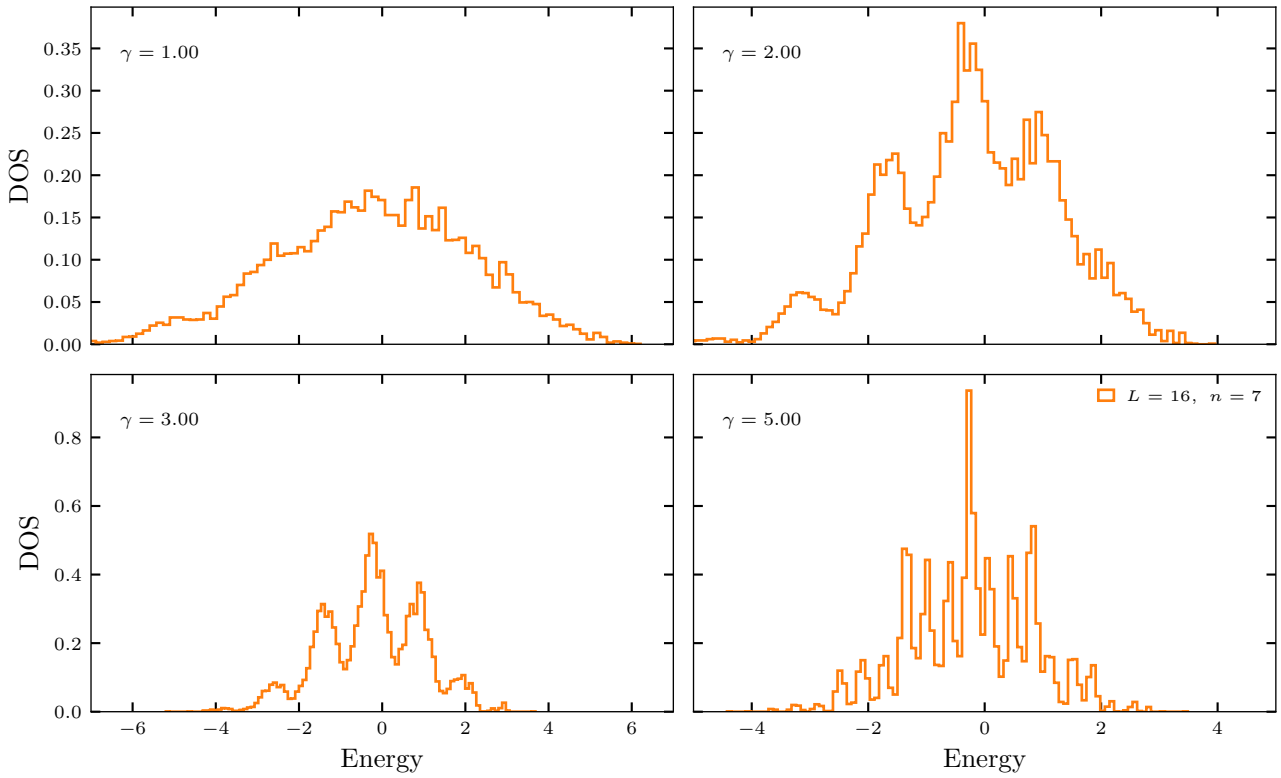

Figure S7. The density of states of the truncated effective Hamiltonian $\hat{H}_{\text{eff}}^{(n=7)}$ for $L = 16$ and $\gamma = 1, 2, 3$ and 5. .All plots were obtained for $J_{xy} = 2,\ J_z = 1$.

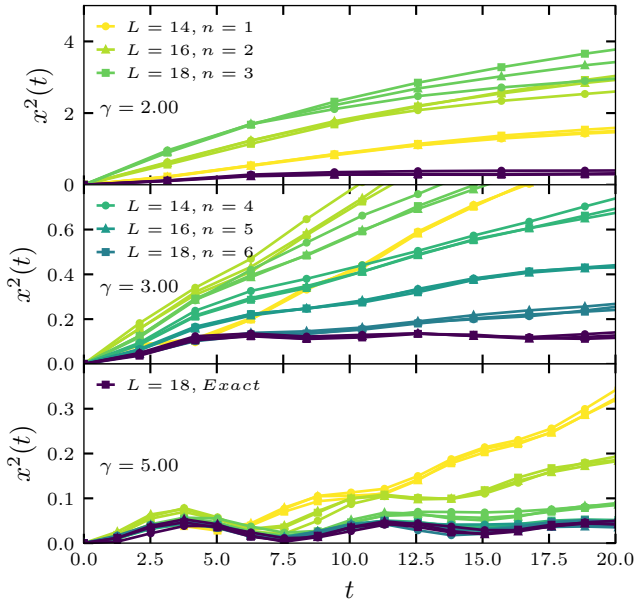

Figure S8. Finite size analysis of Fig. 4 in the main text. Mean-squared displacement as a function of time for various electric fields. The darkest lines correspond to numerically exact results obtained using (Eq. (3) in the main text). The colored lines corresponds to an evolution using the effective Hamiltonian (S2), obtained from a truncated Magnus expansion. Different markers (●, ▲, ■) stand for different system sizes $L = 14, 16$ and 18, correspondingly. The used parameters are, $J_{xy} = 2,\ J_z = 1$.

[1] D. Basko, I. L. Aleiner, and B. L. Altshuler, Metal-insulator transition in a weakly interacting many-electron system with localized single-particle states, Ann. Phys. **321**, 1126 (2006).
[2] I. V. Gornyi, A. Mirlin, and D. Polyakov, Interacting Electrons in Disordered Wires: Anderson Localization and Low-T Transport, Phys. Rev. Lett. **95**, 206603 (2005).
[3] E. Altman and R. Vosk, Universal Dynamics and Renormalization in Many-Body-Localized Systems, Annu. Rev. Condens. Matter Phys. **6**, 383 (2015).
[4] R. Nandkishore and D. A. Huse, Many-Body Localization and Thermalization in Quantum Statistical Mechanics, Annu. Rev. Condens. Matter Phys. **6**, 15 (2015).
[5] R. Vasseur and J. E. Moore, Nonequilibrium quantum dynamics and transport: From integrability to many-body localization, J. Stat. Mech. Theory Exp. **2016**, 064010 (2016).
[6] D. A. Abanin and Z. Papić, Recent progress in many-body localization, Ann. Phys. **529**, 1700169 (2017).
[7] D. A. Abanin, E. Altman, I. Bloch, and M. Serbyn, Colloquium : Many-body localization, thermalization, and entanglement, Rev. Mod. Phys. **91**, 021001 (2019).
[8] D. M. Basko, I. L. Aleiner, and B. L. Altshuler, Possible experimental manifestations of the many-body localization, Phys. Rev. B **76**, 052203 (2007).
[9] M. Ovadia, D. Kalok, I. Tamir, S. Mitra, B. Sacépé, and D. Shahar, Evidence for a Finite-Temperature Insulator, Sci. Rep. **5**, 13503 (2015).
[10] M. Schreiber, S. S. Hodgman, P. Bordia, H. P. Luschen, M. H. Fischer, R. Vosk, E. Altman, U. Schneider, and I. Bloch, Observation of many-body localization of interacting fermions in a quasirandom optical lattice, Science **349**, 842 (2015).
[11] P. Bordia, H. P. Lüschen, S. S. Hodgman, M. Schreiber, I. Bloch, and U. Schneider, Coupling Identical one-dimensional Many-Body Localized Systems, Phys. Rev. Lett. **116**, 140401 (2016).
[12] J. Smith, A. Lee, P. Richerme, B. Neyenhuis, P. W. Hess, P. Hauke, M. Heyl, D. A. Huse, and C. Monroe, Many-body localization in a quantum simulator with programmable random disorder, Nat. Phys. **12**, 907 (2016).
[13] J.-Y. Choi, S. Hild, J. Zeiher, P. Schauss, A. Rubio-Abadal, T. Yefsah, V. Khemani, D. A. Huse, I. Bloch, and C. Gross, Exploring the many-body localization transition in two dimensions, Science **352**, 1547 (2016).
[14] M. Žnidarič, Dephasing-induced diffusive transport in the anisotropic Heisenberg model, New J. Phys. **12**, 043001 (2010).
[15] S. Gopalakrishnan, K. R. Islam, and M. Knap, Noise-Induced Subdiffusion in Strongly Localized Quantum Systems, Phys. Rev. Lett. **119**, 046601 (2017).
[16] A. Lazarides, A. Das, and R. Moessner, Fate of Many-Body Localization Under Periodic Driving, Phys. Rev. Lett. **115**, 030402 (2015).
[17] P. Ponte, Z. Papić, F. Huveneers, and D. A. Abanin, Many-Body Localization in Periodically Driven Systems, Phys. Rev. Lett. **114**, 140401 (2015).
[18] D. A. Abanin, W. De Roeck, and F. Huveneers, Theory of many-body localization in periodically driven systems, Ann. Phys. **372**, 1 (2016).
[19] E. Bairey, G. Refael, and N. H. Lindner, Driving induced many-body localization, Phys. Rev. B **96**, 020201 (2017).
[20] J. Z. Imbrie, On Many-Body Localization for Quantum Spin Chains, J. Stat. Phys. **163**, 998 (2016).
[21] P. W. Anderson, Absence of Diffusion in Certain Random Lattices, Phys. Rev. **109**, 1492 (1958).
[22] R. Nandkishore and A. C. Potter, Marginal Anderson localization and many-body delocalization, Phys. Rev. B **90**, 195115 (2014).
[23] X. Li, S. Ganeshan, J. H. Pixley, and S. Das Sarma, Many-Body Localization and Quantum Nonergodicity in a Model with a Single-Particle Mobility Edge, Phys. Rev. Lett. **115**, 186601 (2015).
[24] X. Li, J. H. Pixley, D.-L. Deng, S. Ganeshan, and S. Das Sarma, Quantum nonergodicity and fermion localization in a system with a single-particle mobility edge, Phys. Rev. B **93**, 184204 (2016).
[25] R. Modak, S. Ghosh, and S. Mukerjee, Criterion for the occurrence of many-body localization in the presence of a single-particle mobility edge, Phys. Rev. B **97**, 104204 (2018).
[26] R. Modak and S. Mukerjee, Many-Body Localization in the Presence of a Single-Particle Mobility Edge, Phys. Rev. Lett. **115**, 230401 (2015).
[27] K. Hyatt, J. R. Garrison, A. C. Potter, and B. Bauer, Many-body localization in the presence of a small bath, Phys. Rev. B **95**, 035132 (2017).
[28] Y. Bar Lev, D. R. Reichman, and Y. Sagi, Many-body localization in system with a completely delocalized single-particle spectrum, Phys. Rev. B **94**, 201116 (2016).
[29] R. Vasseur, A. J. Friedman, S. A. Parameswaran, and A. C. Potter, Particle-hole symmetry, many-body localization, and topological edge modes, Phys. Rev. B **93**, 134207 (2016).
[30] G. Carleo, F. Becca, M. Schiró, and M. Fabrizio, Localization and glassy dynamics of many-body quantum systems, Sci. Rep. **2**, 243 (2012).
[31] M. Schiulaz and M. Müller, Ideal quantum glass transitions: Many-body localization without quenched disorder, in *AIP Conf. Proc.*, Vol. 1610 (American Institute of Physics, 2014) p. 11.
[32] T. Grover and M. P. A. Fisher, Quantum Disentangled Liquids, J. Stat. Mech. Theory Exp. **2014**, P10010 (2013).
[33] M. Schiulaz, A. Silva, and M. Müller, Dynamics in many-body localized quantum systems without disorder, Phys. Rev. B **91**, 184202 (2015).

[34] N. Y. Yao, C. R. Laumann, J. I. Cirac, M. D. Lukin, and J. E. Moore, Quasi-Many-Body Localization in Translation-Invariant Systems, Phys. Rev. Lett. **117**, 240601 (2016).
[35] J. M. Hickey, S. Genway, and J. P. Garrahan, Signatures of many-body localisation in a system without disorder and the relation to a glass transition, J. Stat. Mech. Theory Exp. **2016**, 054047 (2016).
[36] Z. Papić, E. M. Stoudenmire, and D. A. Abanin, Many-body localization in disorder-free systems: The importance of finite-size constraints, Ann. Phys. **362**, 714 (2015).
[37] M. Van Horssen, E. Levi, and J. P. Garrahan, Dynamics of many-body localization in a translation-invariant quantum glass model, Phys. Rev. B **92**, 100305 (2015).
[38] M. Pino, L. B. Ioffe, and B. L. Altshuler, Nonergodic metallic and insulating phases of Josephson junction chains, Proc. Natl. Acad. Sci. **113**, 536 (2016).
[39] D. H. Dunlap and V. M. Kenkre, Dynamic localization of a charged particle moving under the influence of an electric field, Phys. Rev. B **34**, 3625 (1986).
[40] D. Dunlap and V. Kenkre, Dynamic localization of a particle in an electric field viewed in momentum space: Connection with Bloch oscillations, Phys. Lett. A **127**, 438 (1988).
[41] G. H. Wannier, Wave Functions and Effective Hamiltonian for Bloch Electrons in an Electric Field, Phys. Rev. **117**, 432 (1960).
[42] Y. Bar Lev, D. J. Luitz, A. Lazarides, Y. B. Lev, and A. Lazarides, Absence of dynamical localization in interacting driven systems, SciPost Phys. **3**, 029 (2017).
[43] M. Schulz, C. A. Hooley, R. Moessner, and F. Pollmann, Stark Many-Body Localization, Phys. Rev. Lett. **122**, 040606 (2019).
[44] E. van Nieuwenburg, Y. Baum, and G. Refael, From Bloch oscillations to many-body localization in clean interacting systems, Proc. Natl. Acad. Sci. **116**, 9269 (2019).
[45] A. A. Michailidis, M. Žnidarič, M. Medvedyeva, D. A. Abanin, T. Prosen, and Z. Papić, Slow dynamics in translation-invariant quantum lattice models, Phys. Rev. B **97**, 104307 (2018).
[46] S. Pai, M. Pretko, and R. M. Nandkishore, Localization in Fractonic Random Circuits, Phys. Rev. X **9**, 021003 (2019).
[47] V. Khemani, M. Hermele, and R. Nandkishore, Localization from Hilbert space shattering: From theory to physical realizations, Phys. Rev. B **101**, 174204 (2020).
[48] See supplemental material at [URL] for analysis of the spectral statistics, and additional analysis of the magnus expansion.
[49] P. Zhang, Subdiffusion in strongly tilted lattice systems, Phys. Rev. Res. **2**, 033129 (2020).
[50] P. Ribeiro, A. Lazarides, and M. Haque, Many-Body Quantum Dynamics of Initially Trapped Systems due to a Stark Potential: Thermalization versus Bloch Oscillations, Phys. Rev. Lett. **124**, 110603 (2020).
[51] E. V. H. Doggen, I. V. Gornyi, and D. G. Polyakov, Stark many-body localization: Evidence for Hilbert-space shattering, Phys. Rev. B **103**, L100202 (2021).
[52] E. Guardado-Sanchez, A. Morningstar, B. M. Spar, P. T. Brown, D. A. Huse, and W. S. Bakr, Subdiffusion and Heat Transport in a Tilted Two-Dimensional Fermi-Hubbard System, Phys. Rev. X **10**, 011042 (2020).
[53] W. Morong, F. Liu, P. Becker, K. S. Collins, L. Feng, A. Kyprianidis, G. Pagano, T. You, A. V. Gorshkov, and C. Monroe, *Observation of Stark Many-Body Localization without Disorder*, Tech. Rep. (2021).
[54] S. Scherg, T. Kohlert, P. Sala, F. Pollmann, B. Hebbe Madhusudhana, I. Bloch, and M. Aidelsburger, Observing non-ergodicity due to kinetic constraints in tilted Fermi-Hubbard chains, Nat. Commun. **12**, 4490 (2021).
[55] R. Yao, T. Chanda, and J. Zakrzewski, Nonergodic dynamics in disorder-free potentials, Ann. Phys. , 168540 (2021).
[56] P. Jordan and E. Wigner, über das Paulische Äuivalenzverbot, Z. Für Phys. **47**, 631 (1928).
[57] R. Steinigeweg, H. Wichterich, and J. Gemmer, Density dynamics from current auto-correlations at finite time- and length-scales, EPL Europhys. Lett. **88**, 10004 (2009).
[58] Y. Yan, F. Jiang, and H. Zhao, Energy spread and current-current correlation in quantum systems, Eur. Phys. J. B **88**, 11 (2015).
[59] D. J. Luitz and Y. Bar Lev, The ergodic side of the many-body localization transition, Ann. Phys. **529**, 1600350 (2017).
[60] R. Steinigeweg, F. Jin, D. Schmidtke, H. De Raedt, K. Michielsen, and J. Gemmer, Real-time broadening of nonequilibrium density profiles and the role of the specific initial-state realization, Phys. Rev. B **95**, 035155 (2017).
[61] S. Popescu, A. J. Short, and A. Winter, Entanglement and the foundations of statistical mechanics, Nat. Phys. **2**, 754 (2006).
[62] C. Moler and C. Van Loan, Nineteen dubious ways to compute the exponential of a matrix, twenty-five years later, SIAM Rev. **45**, 3 (2003).
[63] U. Schollwöck, The density-matrix renormalization group in the age of matrix product states, Ann. Phys. **326**, 96 (2011).
[64] D. Kennes and C. Karrasch, Extending the range of real time density matrix renormalization group simulations, Computer Physics Communications **200**, 37 (2016).
[65] P. Zhang, Subdiffusion in strongly tilted lattice systems, Phys. Rev. Res. **2**, 33129 (2020).
[66] A. Gromov, A. Lucas, and R. M. Nandkishore, Fracton hydrodynamics, Phys. Rev. Res. **2**, 033124 (2020).
[67] J. Feldmeier, P. Sala, G. De Tomasi, F. Pollmann, and M. Knap, Anomalous Diffusion in Dipole- and Higher-Moment-Conserving Systems, Phys. Rev. Lett. **125**, 245303 (2020).
[68] The entanglement entropy here would be an entanglement of an MPO, which is also not a measurable physical quantity.
[69] D. A. Abanin, W. De Roeck, and F. F. Huveneers, Exponentially Slow Heating in Periodically Driven Many-Body Systems, Phys. Rev. Lett. **115**, 256803 (2015).
[70] D. A. Abanin, W. De Roeck, W. W. Ho, and F. Huveneers, Effective Hamiltonians, prethermalization, and slow energy absorption in periodically driven many-body systems, Phys. Rev. B **95**, 014112 (2017).

[71] D. A. Abanin, W. De Roeck, W. W. Ho, F. Huveneers, W. D. Roeck, W. W. Ho, and F. Huveneers, A Rigorous Theory of Many-Body Prethermalization for Periodically Driven and Closed Quantum Systems, Commun Math Phys **354**, 809 (2017).

[72] S. Blanes, F. Casas, J. A. Oteo, and J. Ros, The Magnus expansion and some of its applications, Phys. Rep. **470**, 151 (2009).

[73] T. Mori, T. Kuwahara, and K. Saito, Rigorous Bound on Energy Absorption and Generic Relaxation in Periodically Driven Quantum Systems, Phys. Rev. Lett. **116**, 120401 (2016).

[74] T. Kuwahara, T. Mori, and K. Saito, Floquet-Magnus theory and generic transient dynamics in periodically driven many-body quantum systems, Ann. Phys. **367**, 96 (2016).